Vietnam Journal of Mechanics, Vol. 46, No. 4 (2024), pp. 331 – 342
DOI: https://doi.org/10.15625/0866-7136/21128

DESIGN OF A TOOTH-SHAPED MAGNETORHEOLOGICAL BRAKE WITH MULTIPLE COILS

Nguyen Van Bien[1], Le Hai Zy Zy[1], Quoc Hung Nguyen[2,*], Ngoc Diep Nguyen[1], Do Qui Duyen[2]

[1]*Department of Mechanical Engineering, Industrial University of Ho Chi Minh City, Vietnam*
[2]*Faculty of Engineering, Vietnamese-German University, Binh Duong Province, Vietnam*
[*]E-mail: hung.nq@vgu.edu.vn

Received: 02 May 2024 / Revised: 28 August 2024 / Accepted: 02 September 2024
Published online: 22 October 2024

Abstract. This research presents an optimized design for a tooth-shaped magnetorheological brake (MRB) with multiple coils. The MRB configuration consists of a disk immersed in magnetorheological fluid (MRF), where four coils act as electromagnets when an electric current is applied. The energized coils induce the alignment of suspended particles in the MRF, forming a chain-like structure that increases the fluid's viscosity. This rapid, strong, and controllable phenomenon enables the MRB to find applications in haptic systems, tension control, and industrial braking systems. To analyze the electromagnetic behavior of the brake, Finite Element Method (FEM) simulations are conducted using ANSYS APDL, and the optimization process is performed utilizing ANSYS Workbench software. The software provides optimized geometries for the brake, resulting in significant improvements in desired performance aspects compared to prior designs, etc.

Keywords: magnetorheological fluid (MRF), magnetorheological brake (MRB), optimal design, ANSYS workbench.

1. INTRODUCTION

Recently, extensive research has been conducted on magnetorheological fluid (MRF) and its wide range of applications. Various devices utilizing MRF, including MR valves, MR brakes, MR clutches, MR dampers, and MR engine mounts, have been the subject of investigation [1, 2]. Among these devices, magnetorheological brakes (MRBs) have garnered significant interest from researchers due to their unique properties and potential applications in different industries. Over the past decade, numerous types of MRBs have been developed, each featuring distinct structural configurations aimed at

achieving higher braking torque, reduced mass or volume, and lower power consumption [3]. These configurations can be categorized into different types, such as disc-type MRBs [4], drum-type MRBs [5], hybrid-type MRBs (combining disc-type and drum-type designs) [6], and MRBs with T-shaped rotors [7]. To enhance the compactness of drum-type MRBs, serpentine flux paths have been implemented [8]. For applications demanding high braking torque, such as automotive engineering, MRBs with multiple-disc rotors have been developed and experimentally validated [9].

In a recent study, Nguyen et al. proposed a novel type of MRB referred to as the side-coil MRB [10]. In this design, magnetic coils are directly placed on the side housings of the MRB. The side-coil configuration addresses several drawbacks associated with traditional MRBs, including magnetic flux "bottle-neck" issues, the need for nonmagnetic bobbins for coil windings, and fabrication complexities. Moreover, optimization results indicated a significant reduction in the mass of the side-coil MRB compared to conventional designs. Subsequently, Nguyen et al. extended their research to side-coil MRBs with thin-wall features on the side housings [11]. The implementation of thin-wall features effectively separates the coils from the working MRF, offering numerous advantages such as smaller achievable gap sizes for the MRF ducts, prevention of contamination of coils, and enhanced convenience for maintenance and testing. Additionally, Nguyen et al. developed MRBs with tooth-shaped rotors [12]. The tooth-shaped cross-section of the rotor enables a larger contact area between the rotor and the working MR fluid, resulting in a compact MRB design with improved performance.

Motivated by the positive outcomes of the tooth-shaped rotor MRB, this research focuses on the further development of tooth-shaped magnetorheological brakes with multiple coils to enhance their performance in terms of braking torque and compactness. The subsequent sections of this paper are structured as follows: Section 2 presents the tooth-shaped MRB with multiple coils, followed by the derivation of its braking torque based on the Bingham rheological model of the MR fluid in Section 3. Section 4 encompasses the optimization of the proposed MRB design and a comparative analysis with previously developed MRBs.

2. CONFIGURATION OF THE TOOTH-SHAPED MRB WITH MULTIPLE COILS

This study introduces a multi-coil tooth-shaped Magnetorheological Brake (MRB) with two teeth and two coils on each side, as depicted in Fig. 1. The MRB comprises housings, a rotating disk featuring two teeth on each side, and a coil positioned above each tooth. The gaps between the disk and housings are filled with Magnetorheological Fluid (MRF). The operational principle of this design can be described as follows: the housings remain stationary while the disk rotates, and the MRF is sheared within the ducts between the housing and the duct. Under zero field conditions, the MRF exists in

its liquid state, displaying a negligible yield strength that has no significant impact on the disk or housings. However, when an electric current is supplied to the coils, the resulting magnetic field begins to influence the iron particles present in the MRF. This leads to their connection and alignment along the magnetic flux lines. Consequently, the MRF within the duct experiences a substantial increase in viscosity, transitioning into a semi-solid state. The enhanced viscosity generates frictional forces acting on the surfaces of both the disk and housings. These frictional forces effectively decelerate and eventually halt the rotation of the disk. The braking moment's magnitude is proportional to the current flowing through the coils. It is noted that counter currents should be applied to the coils to maximize magnetic intensity of the MRB.

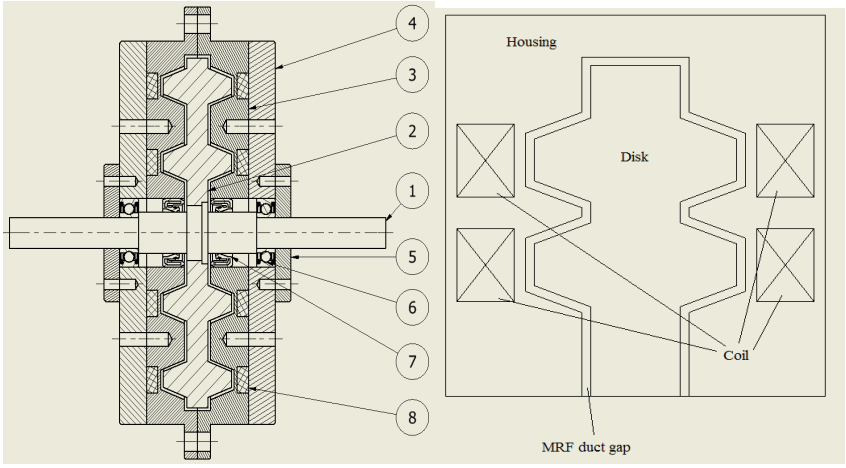

(1)- Shaft, (2)- Brake disk, (3)- Inner Housing, (4)- Outer Housing, (5)- Bearing cover, (6)- Bearing, (7)- Lip-Seal, (8)- Coils

Fig. 1. Configuration of the tooth-shaped MRB with multiple coils

3. BRAKING TORQUE OF THE MRB

The braking torque holds utmost importance as the primary mechanical output measurement for every brake, as it directly determines the brake's effectiveness. A higher braking torque is indicative of superior performance. The objective of brake innovation is to decrease the overall mass and volume while maintaining or even enhancing the required braking torque. In the proposed design of the MR brake, the braking torque is generated throughout the entire MRF slit. To simplify calculations, the MR slit is segmented into various sections, namely straight, cylindrical, and inclined sections. It is assumed that the MRF adheres to the Bingham plastic model, and the velocity of the MRF within the duct is linear. In order to formulate the braking torque of the MRB, firstly the

frictional torque of the MRF in the inclined MRF duct, shown in Fig. 2, is considered. The braking torque in the inclined duct can be determined as follows [12]

$$T = 2\pi L\tau_0 \left(R_i^2 + \frac{1}{3}L^2\sin^2\varphi + R_i L\sin\varphi \right) + \frac{1}{2}\pi\mu\frac{\Omega L}{d}\left(4R^3 + 6R^2 L\sin\varphi + 4R_i L^2\sin^2\varphi + L^3\sin^3\varphi\right). \quad (1)$$

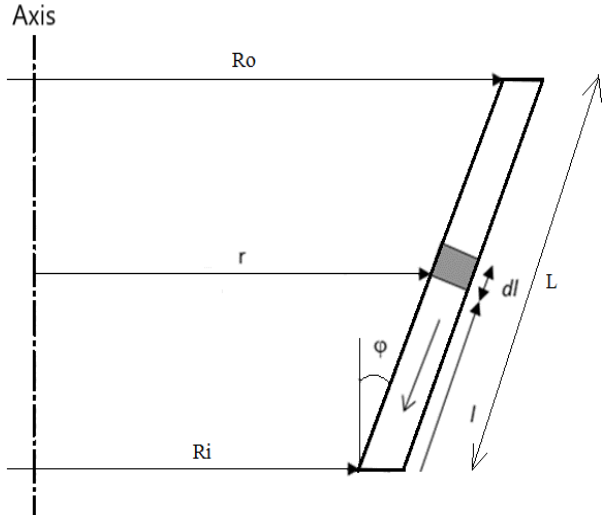

Fig. 2. Geometry of an inclined duct of MRF

It is noted that when φ = 0°, Eq. (1) becomes the equation for calculating torque generated in a cylindrical duct of MRF as follows

$$T_c = 2\pi L_c R_c^2 \left(\tau_c + \frac{\mu\Omega}{d}R_c \right), \quad (2)$$

where L_c is the length of the cylindrical duct; R_c is the radius of the cylindrical duct; d is the gap of the duct; τ_c is the induced yield stress; μ is the post yield viscosity of the MRF and Ω is the angular velocity of the rotor.

When φ = 90°, Eq. (1) becomes the equation for calculating torque generated in an end-face duct of the MRF as follows

$$T_{sj} = \frac{2}{3}\pi\tau_j \left(R_j^3 - R_{j-1}^3 \right) + \frac{\pi\mu\Omega}{2d}\left(R_j^4 - R_{j-1}^4 \right), \quad (3)$$

where τ_j and μ are respectively the shear stress and the post yield viscosity of the MRF in the j-th duct; R_j is the outer radius and R_{j-1} is the inner radius of the duct.

From the above, the braking torque of the MRB can be calculated as follows

$$T_{sj} = \frac{2}{3}\pi\tau_j \left(R_j^3 - R_{j-1}^3 \right) + \frac{\pi\mu\Omega}{2d}\left(R_j^4 - R_{j-1}^4 \right).$$

In the given equation, T_{sj} represents the frictional torque resulting from the MRF in the end-face ducts, as illustrated in Fig. 3. This torque is computed using Eq. (3) mentioned earlier. Tc denotes the frictional torque at the outer cylindrical face of the rotor, which is determined using Eq. (2) with $R_c = R_9$, as depicted in Fig. 3. Lastly, T_{ik} signifies the frictional torque generated in the inclined ducts shown in Fig. 3. The calculation of this torque is determined by the following equation

$$T_{i_k} = 2\pi L\tau_k \left(R_{k-1}^2 + \frac{1}{3}L^2\sin^2\varphi + R_{k-1}L\sin\varphi \right) + \frac{\pi\mu\Omega L}{2d}\left(4R_{k-1}^3 + 6R_{k-1}^2 L\sin\varphi + 4R_{k-1}L^2\sin^2\varphi + L^3\sin^3\varphi\right).$$

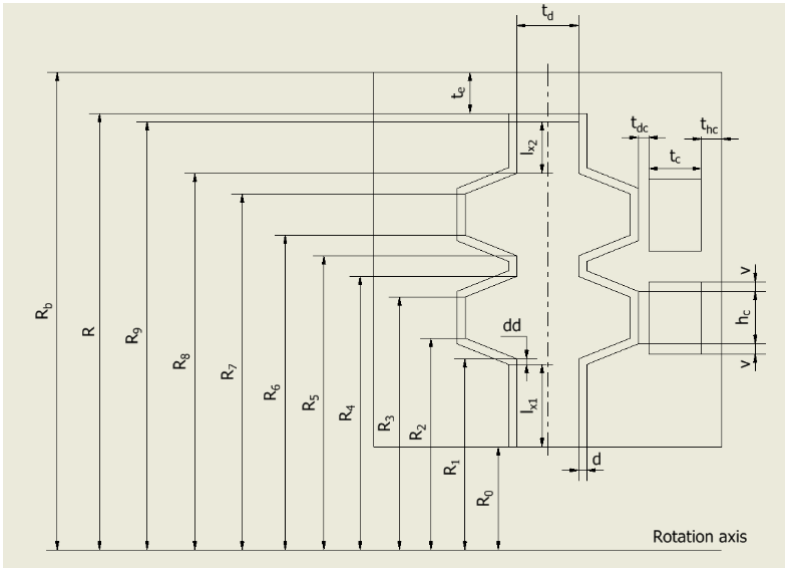

Fig. 3. Details geometric parameters of the MRB

To determine the output torque of the MR brake, two rheological properties of the magnetorheological fluid (MRF) are required: the yield stress and the post-yield viscosity. These properties are influenced by the magnetic flux density passing through the MRF duct and can be approximated as follows [11]

$$\begin{aligned} \tau_{y_i} &= \tau_{y\infty} + \left(\tau_{y_0} - \tau_{y\infty}\right)\left(2e^{-B_i\alpha_{\tau_y}} - e^{-2B_i\alpha_{\tau_y}}\right), \\ \mu_i &= \mu_\infty + \left(\mu_0 - \mu_\infty\right)\left(2e^{-B_i\alpha_\mu} - e^{-2B_i\alpha_\mu}\right), \end{aligned} \tag{4}$$

with τ_{yi}, μ_i are respectively yield the stress and viscosity of path i; τ_{y0}, μ_0 are respectively the yield stress and viscosity of MRF at zero field; $\tau_{y\infty}, \mu_\infty$ are respectively the yield stress and viscosity of MRF at the magnetic saturation; $\alpha_{\tau y}, \alpha_\mu$ are respectively saturation moment index of τ_y and μ_i; B_i is the average magnetic field density of path i. In this study,

the commercial MRF, MRF-132DG, is implemented with the following rheological parameters: $\mu_0 = 0.1$ Pa.s; $\mu_\infty = 3.8$ Pa.s; $\alpha_\mu = 4.5\ \mathrm{T}^{-1}$; $\tau_{y_0} = 15$ Pa; $\tau_\infty = 40000$ Pa; $\alpha_{\tau_y} = 2.9\ \mathrm{T}^{-1}$.

To calculate the induced yield stress using Eq. (4) mentioned previously, it is essential to ascertain the magnetic flux density across the MRF duct. In this research, the magnetic density is determined by employing finite element analysis with the ANSYS APDL software. The finite element model, presented in Fig. 4, incorporates the axisymmetric coupled element, PLANE13, to solve for the magnetic density of the MRB.

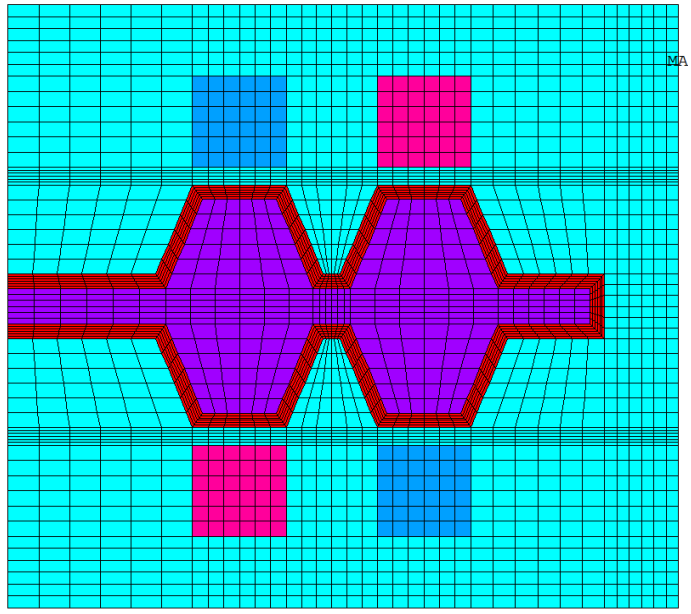

Fig. 4. Finite element model for magnetic circuit analysis of MR brake

4. OPTIMIZATION OF MR BRAKE

In this study, the brake's configuration is constructed using arbitrary design variables. Following that, crucial variables such as the electric current magnitude, current density, wire's cross-sectional diameter, and resistivity are applied to the configuration. The ANSYS APDL software is utilized to perform calculations using the equations outlined in Section 3. Additionally, the same ANSYS APDL software can be utilized to simulate and visualize the results, providing a comprehensive understanding of how the proposed design is influenced by different magnetic flux densities and applied currents. Once the programming phase is completed, the results can be exported to the ANSYS Workbench for the optimization process. This allows for further refinement and

enhancement of the design based on the obtained results and desired objectives. The primary focus in this study is the mechanical output braking torque of the brake, as it is the key determinant of its effectiveness. The objective of the optimization project is to either maximize the braking torque or ensure that it exceeds a specific threshold. Furthermore, to enhance the brake's compatibility, convenience, sustainability, and other aspects, additional factors can be improved upon. Therefore, the optimization work in this study aims to increase the braking torque while simultaneously reducing the mass (or overall volume) of the brake.

Method	Single Objective	Multiple Objectives	Local Search	Global Search	Discrete	Manufacturable Values	Parameter Relationships
Screening		X		X	X	X	X
NLPQL	X		X				X
MISQP	X		X		X	X	X
MOGA		X		X	X	X	X
Adaptive Single-Objective	X			X		X	
Adaptive Multiple-Objective		X		X		X	X
External Optimizer	Capabilities are determined by the optimizer, as defined in the optimization extension.						

Fig. 5. Capabilities of built-in optimization methods

The ANSYS Workbench software provides several built-in optimization methods, each with its own capabilities. These methods offer different approaches to optimization, summarized in Fig. 5, allowing users to choose the most suitable method based on their specific requirements and objectives.

In this study, the boundaries for each input design variable are defined by establishing upper and lower bounds. These bounds are specified within the Domain section of the optimization setup. The study's boundary conditions, which govern the ranges or specific values of the variables, are presented in Table 1.

In this study, the MOGA (Multi-Objective Genetic Algorithm) method is chosen for optimization based on its ability to handle multiple objectives, provide global results, and reveal parameter relationships, as indicated in Fig. 5. It is noted that in the MOGA

Table 1. Design variables and their limits

Design variables	Lower bound (mm)	Upper bound (mm)
Distance between teeth: L_{td}	2	20
Length of tooth top: L_{tt}	3	20
Length of of inclined duct: L_{tx}	2	20
Length of bottom 1: L_{x1}	2	20
Length of bottom 2: L_{x2}	2	20
Number of wire layers: N_{wc}	3 rounds	20
Inner radius: R_0	9	20
Disc thickness: t_d	2	20
Thin-wall: t_{dc}	1	20
Housing thickness 1: t_e	2	20
Housing thickness 2: t_{hc}	2	20
Height of tooth: h_t	5	20

method, selecting the lower and upper bounds for design variables depends on experience, manufacturing capabilities, and the specific requirements of the optimization problem. Setting wide bounds allows for comprehensive and accurate exploration of the solution space, aiding in distinguishing and selecting between local and global optimal solutions. However, a drawback of this approach is the relatively long computational time required for problem-solving. The objective of the optimization is to simultaneously minimize the mass of the brake and maximize the braking torque. To begin the optimization process, a minimum value of 20 Nm is set as the target for the braking torque. This value allows for the inspection and estimation of the feasible mass range for the brake. The objective and constraint sections are then configured to incorporate these two parameters, aligning with their respective objectives and constraints.

Fig. 6 displays the best three candidates from the optimization project, showcasing the values of braking torque and mass for the MR brake. It is noteworthy that the first and second candidate points have a similar ratio of mb/Tb, approximately 0.152 for the first candidate and 0.134 for the second candidate. On the other hand, the third candidate point yields the least optimal result. The similarity in the mb/Tb ratio suggests that the second candidate performed slightly better overall than the first candidate. However, the primary objective of the procedure is to achieve the lowest mass for the brake while maintaining the braking torque above 20 Nm. Despite the slightly lower overall performance, the first candidate point exhibits a significantly lower mass compared to the second candidate point (approximately 0.75 kg less), while still providing sufficient braking torque to meet the predetermined value. Consequently, the design represented by the first candidate point is selected as the best result.

P1 - MB		P2 - TB	
Parameter Value	Variation from Reference	Parameter Value	Variation from Reference
3.8457	-16.06 %	25.341	-25.99 %
4.5812	0.00 %	34.238	0.00 %
4.6909	2.39 %	30.248	-11.65 %

Fig. 6. Capabilities of built-in optimization methods

Furthermore, Fig. 7 provides an illustration of the magnetic flux density distribution of the MR brake with multiple coils at the optimum. The optimal results of the proposed MR brake are summarized in Table 2.

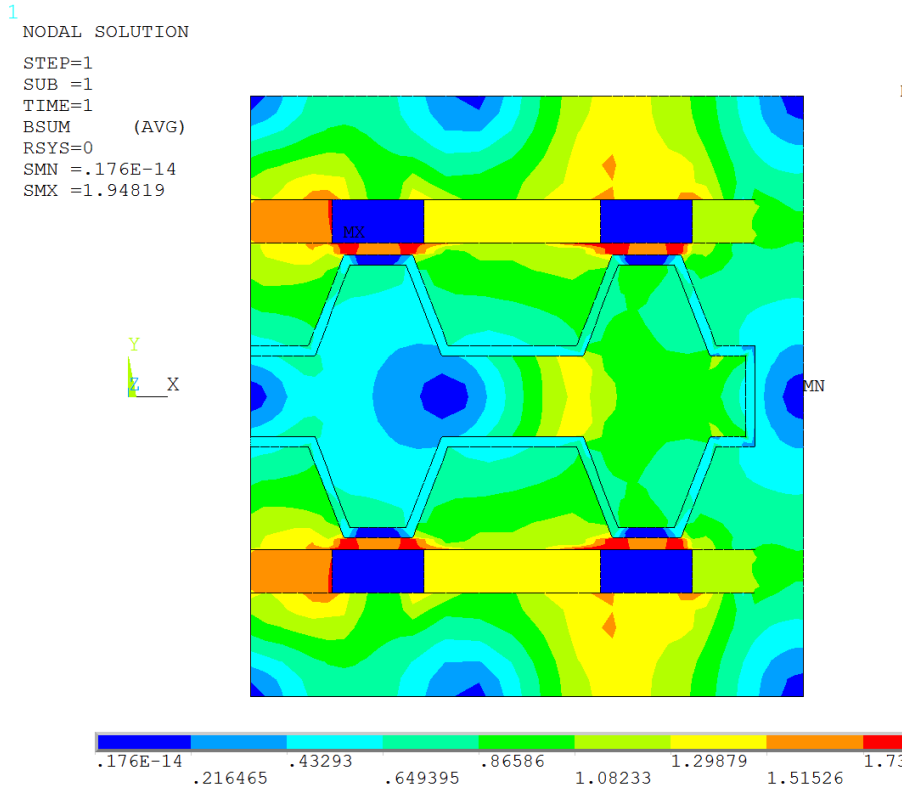

Fig. 7. Magnetic flux density of MR brake with multiple coils at the optimum

Table 2. Optimal results of MR brake with multiple coils

MRB type	Optimal dimensions [mm]	Optimal results
MR brake with tooth-shaped rotor and multiple coils.	Coils: height h_{ct} = 7.606; width t_c = 3.564; number of turns N_c = 73 rounds; Housings: outer radius R_b = 55.86; inner radius R_0 = 10.13; thickness L_b = 49.62; Disk: thickness t_d = 6.71; tooth height h_t = 7.51; tooth-top length L_{tt} = 4.62; tooth inclined length L_{ti} = 8.06; inclined angle = 1.2 rad; teeth distance L_{td} = 11.72; MRF duct gap: d = 0.8.	Braking torque: 25.341 Nm; Mass: 3.85 kg; Current: 2.5 A; Power consumption: 32.28 W.

The obtained and discussed results of the proposed MR brake optimization design are compared with those of the previous tooth-shaped single-coil MR brake design. The objective of this study is to assess whether the proposed optimal design exhibits superiority in desired aspects when compared to other designs. The specific design chosen for comparison is the tooth-shaped MR brake with a single coil [12]. Using the same configuration and design variables, the MR brake with a single coil is evaluated and optimized to achieve its optimal design. The results of the optimal design for the single-coil MR brake are presented in Fig. 8. A comparison between the tooth-shaped MR brake with a single coil and the tooth-shaped MR brake with multiple coils reveals that the former provides less braking torque and has a heavier mass. Specifically, the tooth-shaped MR brake with a single coil generates a braking torque of 21.146 Nm with a mass of 4.93 kg, whereas the tooth-shaped MR brake with multiple coils achieves a higher braking torque of 25.341 Nm with a lower mass of 3.85 kg. Considering that the density of the brake's material remains unchanged, a lighter mass corresponds to a smaller volume for the brake. Consequently, the optimal design of the tooth-shaped MR brake with multiple coils surpasses its predecessor in all three aspects: braking torque generated, mass, and volume. Moreover, Fig. 9 depicts the relationship between braking torque and mass for the two proposed MR brakes. It clearly shows that the MR brake with multiple coils consistently produces more braking torque for a given brake mass. Therefore, it can be concluded that the tooth-shaped MR brake with multiple coils is superior to the one with a single coil.

P7 - MB		P14 - TB	
Parameter Value	Variation from Reference	Parameter Value	Variation from Reference
✕✕ 4.93	0.00 %	21.146	0.00 %

Fig. 8. Optimal results of tooth-shaped MR brake with single coil

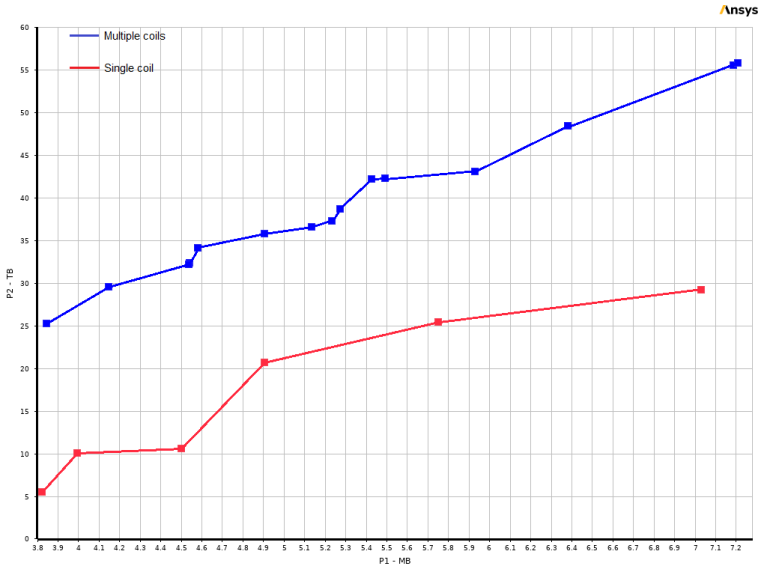

Fig. 9. Relationships between torque and mass of two proposed MR brakes

5. CONCLUSIONS

In conclusion, the research presents an optimal design for the Magnetorheological Fluid Brake (MRB) by utilizing a tooth-shaped MRB with multiple coils. The design showcases superiority over the previous tooth-shaped MRB with a single coil, demonstrating reduced weight and increased braking torque generation. The working principle and configuration of the MRB are explained, employing the Bingham plastic rheological model of Magnetorheological Fluid (MRF) and finite element analysis. A mathematical model for braking torque is developed, and an optimization problem is formulated to minimize the mass of the proposed MRB. The optimization problem includes a constraint to ensure that the output brake torque is greater than or equal to the desired torque of 20 Nm. The optimal results of the tooth-shaped MRB with multiple coils indicate a mass of 3.85 kg and an output brake torque of 25.341 Nm. However, it is important to note that factors such as durability, compatibility, and life expectancy of the MRB have not been extensively investigated in this study. Therefore, further research is recommended to explore and address these aspects to fully implement and optimize the proposed MRB design.

DECLARATION OF COMPETING INTEREST

The authors declare that they have no known competing financial interests or personal relationships that could have appeared to influence the work reported in this paper.

ACKNOWLEDGEMENT

This work was supported by a research fund from the Ministry of Education and Training (MOET) of Vietnam under the grand no. B2022-VGU-02.

REFERENCES

[1] Q.-D. Bui, Q. H. Nguyen, and L.-V. Hoang. A control system for MR damper-based suspension of front-loaded washing machines featuring magnetic induction coils and phase-lead compensator. *Journal of Intelligent Material Systems and Structures*, **34**, (2022), pp. 631–641. https://doi.org/10.1177/1045389x221117492.

[2] K. Kluszczyński and Z. Pilch. The choice of the optimal number of discs in an MR clutch from the viewpoint of different criteria and constraints. *Energies*, **14**, (2021). https://doi.org/10.3390/en14216888.

[3] G. Hu, L. Wu, and L. Li. Torque characteristics analysis of a magnetorheological brake with double brake disc. *Actuators*, **10**, (2021), p. 23. https://doi.org/10.3390/act10020023.

[4] N. D. Nguyen, T. Le-Duc, L. D. Hiep, and Q. H. Nguyen. Development of a new magnetorheological fluid–based brake with multiple coils placed on the side housings. *Journal of Intelligent Material Systems and Structures*, **30**, (2018), pp. 734–748. https://doi.org/10.1177/1045389x18818385.

[5] H. Qin, A. Song, X. Zeng, and S. Hu. Design and evaluation of a small-scale multi-drum magnetorheological brake. *Journal of Intelligent Material Systems and Structures*, **29**, (2018), pp. 2607–2618. https://doi.org/10.1177/1045389x18770878.

[6] Q. H. Nguyen and S. B. Choi. Selection of magnetorheological brake types via optimal design considering maximum torque and constrained volume. *Smart Materials and Structures*, **21**, (2011). https://doi.org/10.1088/0964-1726/21/1/015012.

[7] N. Q. Hung and C. S. Bok. Optimal design of a T-shaped drum-type brake for motorcycle utilizing magnetorheological fluid. *Mechanics Based Design of Structures and Machines*, **40**, (2012), pp. 153–162. https://doi.org/10.1080/15397734.2011.616479.

[8] Q. H. Nguyen, V. B. Nguyen, H. D. Le, D. Q. Duyen, W. Li, and N. X. Hung. Development of a novel magnetorheological brake with zigzag magnetic flux path. *Smart Materials and Structures*, **30**, (2021). https://doi.org/10.1088/1361-665x/ac3430.

[9] Q. H. Nguyen and S. B. Choi. Optimal design of an automotive magnetorheological brake considering geometric dimensions and zero-field friction heat. *Smart Materials and Structures*, **19**, (2010). https://doi.org/10.1088/0964-1726/19/11/115024.

[10] N. V. Quoc, L. D. Tuan, L. D. Hiep, H. N. Quoc, and S. B. Choi. Material characterization of MR fluid on performance of MRF based brake. *Frontiers in Materials*, **6**, (2019). https://doi.org/10.3389/fmats.2019.00125.

[11] N. D. Nguyen, T. T. Nguyen, D. H. Le, and Q. H. Nguyen. Design and investigation of a novel magnetorheological brake with coils directly placed on side housings using a separating thin wall. *Journal of Intelligent Material Systems and Structures*, **32**, (2021), pp. 1565–1579. https://doi.org/10.1177/1045389x21993912.

[12] V. B. Nguyen, H. D. Le, Q. H. Nguyen, D. Q. Duyen, D. H. M. Hieu, and S.-B. Choi. Design and experimental evaluation a novel magneto-rheological brake with tooth shaped rotor. *Smart Materials and Structures*, **31**, (2021). https://doi.org/10.1088/1361-665x/ac38ff.